PROCEEDINGS

55. IWK

Internationales Wissenschaftliches Kolloquium
International Scientific Colloquium

13 - 17 September 2010

Crossing Borders within the ABC

Automation,

Biomedical Engineering and

Computer Science

Faculty of
Computer Science and Automation

www.tu-ilmenau.de

TECHNISCHE UNIVERSITÄT
ILMENAU

Impressum
Published by

Publisher: Rector of the Ilmenau University of Technology
Univ.-Prof. Dr. rer. nat. habil. Dr. h. c. Prof. h. c. Peter Scharff

Editor: Marketing Department (Phone: +49 3677 69-2520)
Andrea Schneider (conferences@tu-ilmenau.de)

Faculty of Computer Science and Automation
(Phone: +49 3677 69-2860)
Univ.-Prof. Dr.-Ing. habil. Jens Haueisen

Editorial Deadline: 20. August 2010

Implementation: Ilmenau University of Technology
Felix Böckelmann
Philipp Schmidt

USB-Flash-Version.

Publishing House: Verlag ISLE, Betriebsstätte des ISLE e.V.
Werner-von-Siemens-Str. 16
98693 Ilmenau

Production: CDA Datenträger Albrechts GmbH, 98529 Suhl/Albrechts

Order trough: Marketing Department (+49 3677 69-2520)
Andrea Schneider (conferences@tu-ilmenau.de)

ISBN: 978-3-938843-53-6 (USB-Flash Version)

Online-Version:

Publisher: Universitätsbibliothek Ilmenau
ilmedia
Postfach 10 05 65
98684 Ilmenau

Home / Index:
http://www.db-thueringen.de/servlets/DocumentServlet?id=16739

MODELLING AND IDENTIFICATION OF A HIGH-PRECISION PLANAR POSITIONING SYSTEM

Kai Treichel, Kai Wulff, Johann Reger

Ilmenau University of Technology
Control Engineering Group
P.O. Box 10 05 65
D-98684, Ilmenau, Germany

Stefan Amthor

TETRA Gesellschaft für Sensorik,
Robotik und Automation mbH
Gewerbepark Am Wald 4
D-98693 Ilmenau, Germany

ABSTRACT

This contribution is dedicated to developing a thorough physical model of a high-precision planar positioning system. Subject of this investigation is Tetra's state-of-the-art high-precision planar positioning system "PPS200" using air bearings and electromagnetic coupling as a principle of propulsion. We develop physical models of all components and investigate the influence of various physical effects. The model characteristics and parameters are identified using experimental data taken from the dedicated test rig. The resulting system is implemented as a simulation model and verified by measurements of several experiments conducted at the test rig.

***Index Terms*—** planar positioning system, air bearing, electro magnetic propulsion, physical modelling

1. INTRODUCTION

In order to meet the increasing requirements in high performance and high dimension accuracy for positioning systems, there has been active research on hovering, high-precision planar positioning systems in the past few years [1], [2], [3], [4], [5]. While latest technology provides precise positioning capabilities down to the Nanometer scale, further improvements in high-precision dynamic positioning will only be possible by applying modern nonlinear control methods. This contribution constitutes the first step towards this ambitious goal by providing a detailed mathematical model of Tetra's state-of-the-art planar positioning system "PPS200".

The "PPS200" system consists of a stator base and a slider which is levitated over the stator plate by means of air bearings. The slider is suitable to carry a maximal pay load of $14kg$ which is to be positioned in the plane with a specified yaw-angle. The travel range of the slider is 200x200mm^2 and the maximal yaw angle is $\pm 0.25°$. A number of permanent magnets are mounted at the bottom of the slider. Those magnets are hovering above rigidly fixed current-carrying conductors embedded into the stator plate. Currents through those conductors together with the permanent magnets generate a force between the stator plate and the slider resulting in an acceleration of the slider (see [6] for a discussion on the concept of construction).

Controlling the position of the slider (or even following predefined trajectories) to the highest degree of precision is challenged by serval nonlinear dynamics of the system's components. Moreover, at a certain degree of precision characteristics such as ripples caused by PWM amplifier or parasitic capacities may be relevant for the dynamical behaviour of the system. In order to take the precision of the control onto such a level, a detailed physical model of the dynamics is needed. The goal of this contribution is to develop such a model and to provide some insights into possible relevant effects.

The paper is structured as follows. In the next section we give an overview of the structure and introduce the main components of the positioning system. A detailed model of the actuator is developed in Section 3 followed by a discussion on the electromechanical coupling in Section 4. In Section 5 we present the mechanical model of the slider considering 6 degrees of freedom. The simulation results of the developed model are verified and compared with the measurements from the test rig in Section 6.

Contact: {kai.treichel, kai.wulff, johann.reger}@tu-ilmenau.de

2. THE PPS200 STRUCTURE

The "PPS200" positioning system is an electromechanical drive composed of two main elements: an aerostatic guided slider carrying the load to be positioned and a stator plate with imbedded coils (c.f. Fig. 1). The slider is hovering on air-bearings above the stator plate providing nearly frictionless motion. The coils functional complements are permanent magnets mounted at the bottom of the slider such that their magnetic field interacts with the current through the coils of the stator plate resulting in a force (Lorentz-force) which consequently propels the slider. The position driven is measured by an optical, incremental measurement system consisting of two parts – a measurement grid which is directly located at the bottom of the slider at its center of gravity and a sensor system composed of three optical sensors located at the center of the stator plate [5]. One sensor is used to measure motion in the direction of x and the rest of them being y_1 and y_2 are used in order to compensate or even actively control the yaw ϕ_z along the vertical z axis as well as detecting the y-position driven. Unsurprisingly other positioning systems share similar assemblies [4].

In order to capture the slider's motion an earth-fixed coordinate system (x, y, z) located at the center of the stator plate is used. The coordinates x and y describe the position of the slider's center of gravity, while ϕ_z denotes the slider's orientation or yaw.

The block-diagram in Fig. 2 shows the basic structure of the closed loop system. The aim is to control the slider coordinates (x, y, ϕ_z) measured by the sensor system described, via the current through the coils considered as control input. Therefore the variables (x_d, y_d, ϕ_{z_d}) define the reference trajectory for the slider to travel.

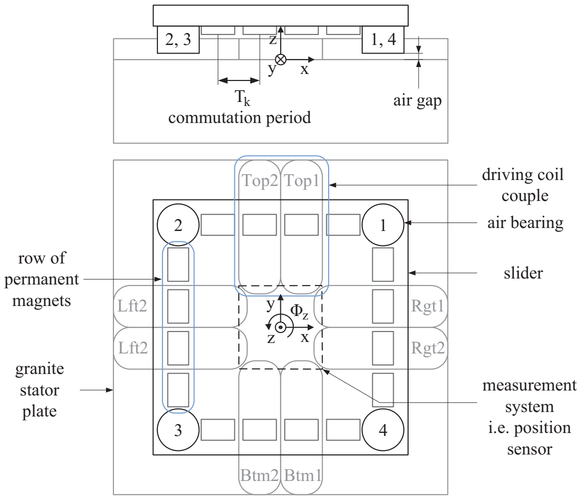

Fig. 1. Basic assembly of the positioning system

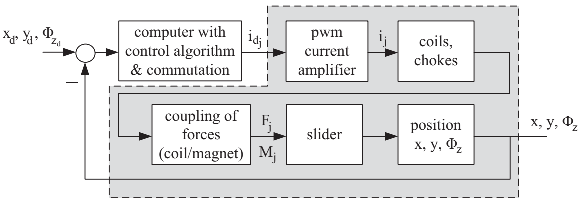

Fig. 2. Block-structure of the PPS200 positioning system

These reference values are fed into the controller which generates an actuator signal being the desired current vector $\mathbf{i_d} = (i_{d_x}\ i_{d_y}\ i_{d_{\phi_z}})^T$. $\mathbf{i_d}$ is then fed into a commutation function which separates the currents position dependent on the actuating element.

The actuating element is composed of j PWM-amplifiers connected to the j driving coils, where $j \in \{Btm_1, Btm_2, Rgt_1, Rgt_2, Top_1, Top_2, Lft_1, Lft_2\}$ represents the coil denotation. Chokes in series before and behind each driving coil are used to ensure EMC compatibility. Accordingly the currents i_j through the coils are the actuator signals or control inputs. These currents are transformed into the Lorentz-forces F_j via the coupling of forces between coils and permanent magnets thus actuating the slider (plant) and its position (x, y, ϕ_z). The forces applied between the permanent magnets and the bottom and top coil couple will move the slider in the direction of x, while by interaction between the magnets and the left and right coil couple the slider will move in the direction of y. The slider's acceleration and thus the total force acting on the slider is proportional to the currents applied. Since the slider is levitated it will also experience a suspension z, roll θ_x and pitch ψ_y. Hence, the slider's states are x, y, z, θ_x, ψ_y and ϕ_z.

3. ELECTRICAL PWM CURRENT AMPLIFIER AND DRIVING COIL MODEL

The slider is driven by eight actuators each consisting of a PWM amplifier and a driving coil. In this section we investigate the dynamics of these actuators. For simplicity of notation we shall omit the index j denoting the location of the respective actuator in this section.

The PWM-amplifier is especially designed by the IMMS[1] to match the requirements of the "PPS200". In order to model the amplifier, we extracted its basic structure from its electrical circuit which can be seen in Fig. 3. It basically consists of

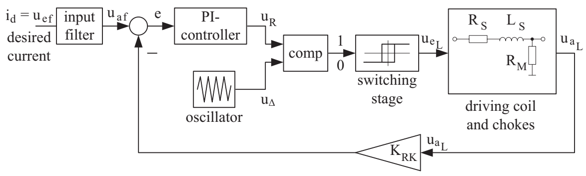

Fig. 3. Basic structure of one of the eight PWM-current-amplifiers

an input filter determining the cut-off frequency of the input signal, a controller to control the current i through the load to the desired set point specified by the input signal i_d, a triangle wave form oscillator in conjunction with a comparator to modulate the actuator signal of the controller to a PWM-signal and a switching stage composed of power transistors in switching mode amplifying the PWM-signal. The load is connected in an H-bridge, while the current through the load is measured through the voltage across the measuring resistance R_M and fed back to the controller in order to track the desired value.

The desired current through the coils i_d is represented by the voltage u_{ef} across the input filter which is a simple RC-low-pass filter. It can be described by

$$\dot{u}_{af}(t) = \frac{1}{T_f}\,(u_{ef}(t) - u_{af}(t)), \tag{1}$$

where $T_f = RC$ is the lag time constant. After filtering, the desired set point for the current through the coil is denoted by the voltage u_{af} being the input for the PI-controller which generates the actuator signal u_R, also measured in volts. The control law for the PI-controller is given by

$$u_R(t) = K_R\left(e(t) + \frac{1}{T_{nR}}\int_0^t e(\tau)d\tau\right). \tag{2}$$

K_R and T_{n_R} denote the controller gain and the time constant of the integrator, respectively. The control error is

$$e(t) = u_{af}(t) - K_{RK}\,u_{a_L}(t). \tag{3}$$

In the comparator unit (denoted "comp" in Fig. 3) the signal u_R is compared to a triangle wave form u_Δ with a base frequency of roughly 22 kHz. Thus the output of the comparator switches to high, if $u_R > u_\Delta$ or to low, if $u_R < u_\Delta$ generating the pulse width modulated signal with respect to the desired input signal. This signal is amplified by power MOSFETs operating in switching mode (see switching stage in Fig. 3). The amplifiers output is given by the piecewise constant function

$$u_{eL}(t) = \begin{cases} +u_{e_{L_{max}}} & \text{for} \quad u_R(t) > u_\Delta(t) \\ -u_{e_{L_{max}}} & \text{for} \quad u_R(t) < u_\Delta(t) \end{cases}, \tag{4}$$

where $u_{e_{L_{max}}} = 150V$.

The second part of the actuator consists of the driving coils and two further coils in series acting as chokes for improving EMC. The resistance R_S in Fig. 3 represents the sum

[1] Institut für Mikroelektronik- und Mechatronik-Systeme gGmbH, Ilmenau

of the coil winding resistances of those three coils and L_S denotes their overall inductance. Finally R_M is a resistance to ground used to measure the current through the coils. The amplified pulse width modulated signal u_{e_L} acts at the input of this network. The dynamics of this circuit is given by:

$$\frac{di(t)}{dt} = -\frac{1}{L_S}\Big((R_M + R_S)i(t) - u_{eL}(t)\Big). \quad (5)$$

The output voltage $u_{a_L} = R_M i$ is fed back via the gain K_{RK} in the feedback loop.

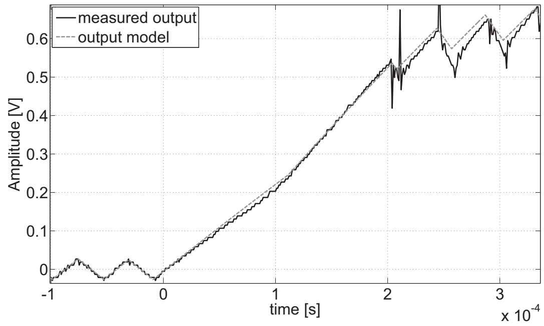

(a)

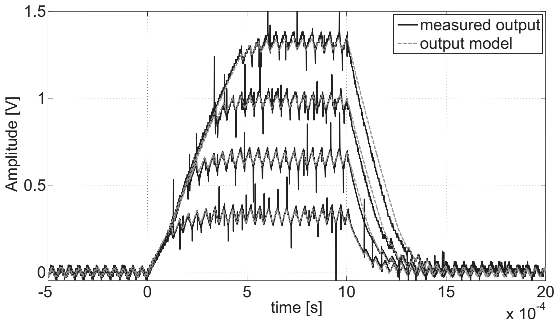

(b)

Fig. 4. Comparison of measurements and simulation of the actuator model using the nonlinear inductance (6) ($100mV \hat{=} 1A$). (a) Detail of the slope. (b) Step responses for input signals of 1-4V.

For verification of the derived model we conducted several experiments at the test rig. At the input of the PWM-amplifier we applied rectangular pulse signals with amplitudes varying between 1 and 4V while the slider was removed. The current i through the coils was measured with a clamp-on ammeter.

Fig. 4 (b) shows the measured data for different amplitudes, where $100mV \hat{=} 1A$. Besides the ripples that are characteristic for a PWM-amplifier at constant currents, we can observe a significant increase of the slope when the current exceeds 2A, c.f. the detail in Fig 4 (a). This slope increase cannot be reproduced using the linear model of the coils in equation (5). In fact, this nonlinear behaviour is due to magnetic saturation of the metal core of the driving coil. At a certain current i_{sat}, called saturation current, the permeability of the core decreases. This leads to a loss of inductance of the coils until eventually the coil behaves like an air-core coil. Thus, the inductance of the coils L_S is to be modelled as a nonlinear function of the current $i(t)$. To approximate this nonlinear behaviour of the inductance we choose the following approach:

$$L_S(i(t)) = K_1 \arctan(K_2\,|i(t)| + K_3) + K_4\,. \quad (6)$$

The Parameters $K_1, \ldots, K_4$ were obtained by standard nonlinear least-squares optimization.

In Fig. 4 the measured data is compared to the simulation using the nonlinear inductance model (6). The overall performance of the model is very satisfying and even that characteristic increase of the slope due to core saturation (c.f. Fig 4 (a)) is very well matched.

4. ELECTROMECHANICAL COUPLING

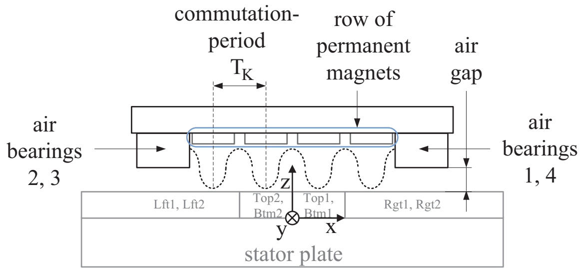

Fig. 5. Shape of the magnetic field of the permanent magnets along the x axis

The forces acting on the slider are generated by the interaction between the electromagnetic field induced by the current through the driving coils and the magnetic field of the permanent magnets at the bottom of the slider. According to Lorentz' law the electromagnetic force is given by

$$\mathbf{F_L} = i\mathbf{l} \times \mathbf{B}, \quad (7)$$

where i is the current through a wire with constant length $\mathbf{l}$ and $\mathbf{B}$ is the flux density of the homogeneous magnetic field of a permanent magnet [7].

In order to derive a sufficiently precise description of the electromagnetic coupling we make the following (mild) assumptions:

1. *The vertical distance between the magnets and the coil-surface is sufficiently small so that the magnetic field is homogeneous (in the vertical direction) and perpendicular with respect to the coil surface.*
2. *The sag (subsidence) of the air bearings (roughly 5 μm) is coupled with the quantities z, θ_x and ψ_y of the slider. The influence of these quantities on the absolute value as well as the direction of the Lorentz-force is negligibly small. Hence, we assume that the magnetic field is always perpendicular to every single coil-winding such that the forces for the x- and y-direction are decoupled from each other. The forces act always perpendicular with respect to the corresponding driving coil regardless of the orientation of the slider.*
3. *The rotation about the z-axis is sufficiently small such that the electromagnetically relevant area between the magnets and the coils' surfaces is independent of the slider's orientation ϕ_z. In fact the maximum rotation is restricted to $\phi_{z,max} = \pm 0.25°$.*

With the above assumptions the electromagnetic force generated by the j-th coil and the slider's magnetic field is given by

$$F_j = i_j l B\,, \tag{8}$$

where i_j is the current through the respective coil, l is the effective length of the conductor and B is the magnetic flux density of the magnetic field effective for the coil.

The magnetic field generated by the magnets is not homogeneous along the x-axis (bottom and top coils) and the y-axis (left and right coils), see Fig. 5 for an illustration. Thus the flux density B of the magnetic field interacting with the coils depends on the slider position above the stator plate. Fig. 6 shows the measurements of the magnetic flux over the x-position of the slider. Approximating this function by

$$B_x = \hat{B}\cos\left(\frac{2\pi}{T_K}x\right) \tag{9}$$

where T_K is the distance between the centers of adjacent magnets, yields satisfying results as shown also in Fig. 6.

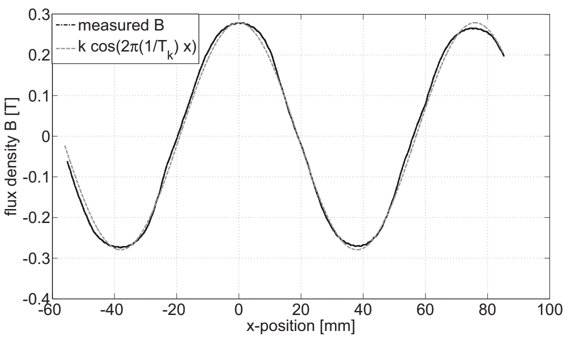

Fig. 6. Magnetic flux density along the x-direction.

In order to compensate for the spacial dependency of the magnetic field we consider the structure depicted in Fig. 7 (suggested in [6]). The inputs are the desired forces in x- and y-direction and rotation torque expressed by $(i_{d_x}, i_{d_y}, i_{d_{\phi_z}})$, respectively. The outputs are the resulting forces F_x, F_y and the torque M_z acting on the slider.

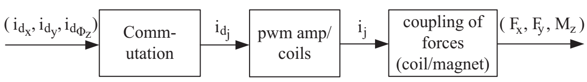

Fig. 7. Feedforward-structure to compensate the spacial dependance of the magnetic field.

The resulting force on the slider in x- direction is given by

$$F_x = F_{Top1} + F_{Top2} + F_{Btm1} + F_{Btm2}\,. \tag{10}$$

By choosing the currents i_{d_j} as sinusoidal functions of the slider position x with appropriate phase-shift accounting for the offsets due to the coil position on the stator, the spacial dependency can be compensated by the commutation. Assuming an ideal compensation yields for the force on the slider:

$$F_x = 2l\hat{B}\, i_{d_x}\,, \tag{11}$$

where l in $[m]$ is the effective length of the conductor and $\hat{B}$ is the magnitude of the magnetic flux density in $[T]$. Note, that $l\hat{B}$ is constant such that the force F_x only depends on the current i_{d_x}, but is independent of the slider's position. Similar considerations yield according results for F_y and M_z.

5. MECHANICAL SLIDER MODEL

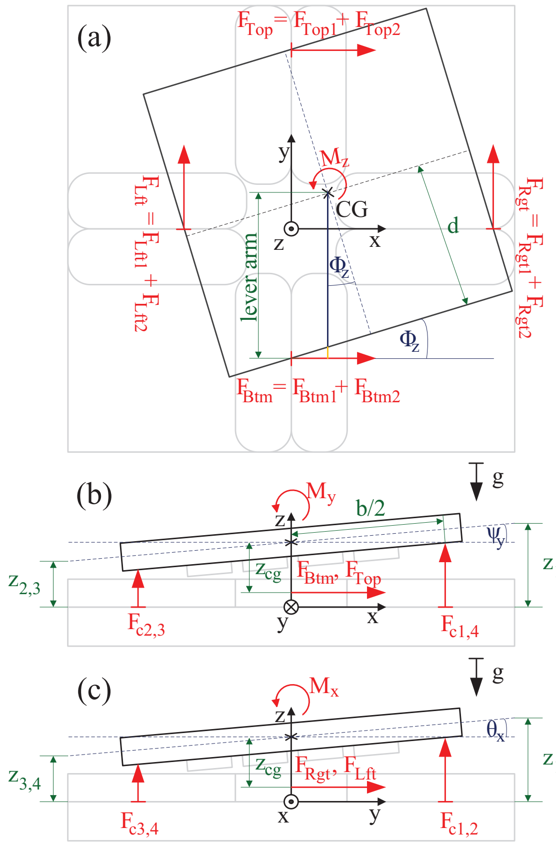

Fig. 8. Planar (a) and vertical (b),(c) forces as well as torque along the x (c), y (b) and z (a) axes (red:forces and torque, blue:angles, green:distances)

The slider is essentially a mass with six degrees of freedom suspended by air bearings. Deriving the equations of motion we shall distinguish between the planar movements (x, y, ϕ_z) and the additional spacial movements (z, θ_x, ψ_y) considering the third dimension. In the former case the prominent forces on the slider are the propelling electromagnetic forces and some viscous friction forces due to the air bearings. In the latter case, the slider motion is dominantly influenced by the suspending forces, but we shall also consider the fact that the propelling forces attack outside the center of gravity and thus cause for roll and pitch motion.

To begin with we derive the planar equations of motion, see Fig. 8 (a). The black square in the figure denotes the points of attack of the electromagnetic forces along the rows of permanent magnets at the bottom of the slider. Assuming that the planar forces are decoupled (see Section 4) we obtain the following balance of forces by applying the principle of linear momentum (Newton's second law):

$$m\ddot{x} = F_{Btm} + F_{Top} - F_{R_x} \tag{12}$$
$$m\ddot{y} = F_{Rgt} + F_{Lft} - F_{R_y}\,, \tag{13}$$

where m is the slider mass and $F_{Btm}, F_{Top}, F_{Rgt}, F_{Lft}$ are the resulting forces of each respective pair of coils. The linear damping terms $F_{R_x} = k_r\dot{x}$ and $F_{R_y} = k_r\dot{y}$ denote the so-called drag- or viscous friction forces (Stokes law) evoked by the air bearings and the viscosity of air (see [2]).

For the motion about the z-axis we apply the principle of conservation of angular momentum:

$$J_{z_{CG}} \ddot{\phi}_z = M_{z_{Btm}} + M_{z_{Rgt}} - M_{z_{Top}} - M_{z_{Lft}}\,, \quad (14)$$

where $J_{z_{CG}}$ denotes the slider's moment of inertia about the z-axis and the respective torques are given by

$$M_{z_{Btm}} = \Big(\frac{d}{\cos(\phi_z)} + x\tan(\phi_z)\Big) F_{Btm} \quad (15)$$

$$M_{z_{Top}} = \Big(\frac{d}{\cos(\phi_z)} - x\tan(\phi_z)\Big) F_{Top} \quad (16)$$

$$M_{z_{Rgt}} = \Big(\frac{d}{\cos(\phi_z)} + y\tan(\phi_z)\Big) F_{Rgt} \quad (17)$$

$$M_{z_{Lft}} = \Big(\frac{d}{\cos(\phi_z)} - y\tan(\phi_z)\Big) F_{Lft} \quad (18)$$

For the dynamics in z-direction we are investigating the influence of the air bearings. The air bearings are vacuum preloaded meaning that they provide vacuum air as well as pressurisation (see [8]). We approximate their dynamical behaviour with a simple parallel spring-damper model similar to the approach in [3]. The suspension force F_{c_i} of the i-th air bearing is then given by

$$F_{c_i} = c_{ll} z_i - d_{ll} \dot{z}_i \quad (19)$$

where d_{ll} is the damping-constant, z_i is the distance between the stator surface and the i-th air bearing, and c_{ll} is the spring constant which again depends on the air gap z_i. Elementary geometric considerations (c.f. Fig. 8 (b),(c)) yield for the air gaps at each bearing:

$$z_1 = z + \frac{b}{2}\Big(\sin(\theta_x) + \sin(\psi_y)\Big) \quad (20)$$

$$z_2 = z + \frac{b}{2}\Big(\sin(\theta_x) - \sin(\psi_y)\Big) \quad (21)$$

$$z_3 = z - \frac{b}{2}\Big(\sin(\theta_x) - \sin(\psi_y)\Big) \quad (22)$$

$$z_4 = z - \frac{b}{2}\Big(\sin(\theta_x) + \sin(\psi_y)\Big) \quad (23)$$

For identification of the spring constant c_{ll} we resort to extensive experiments conducted at the IMMS who established a typical load deflection curve of an air bearing depicted in Fig. 9. Note however, that for a particular air bearing this curve may differ significantly.

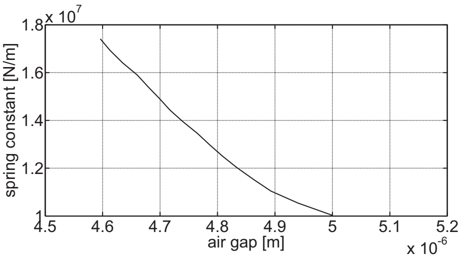

Fig. 9. Load deflection curve of a single air bearing established by the IMMS

The dynamics in the z-direction are then given by

$$m\ddot{z} = \sum_{i=1}^{4} F_{c_i} - mg\,. \quad (24)$$

Finally we consider the balances of torques about the x- and y-axis:

$$J_{x_{CG}} \ddot{\theta}_x = z_{cg}\Big(F_{Rgt} + F_{Lft}\Big) + \\ + \frac{b}{2}\Big(F_{c_1} + F_{c_2} - F_{c_3} - F_{c_4}\Big) \quad (25)$$

$$J_{y_{CG}} \ddot{\psi}_y = z_{cg}\Big(F_{Btm} + F_{Top}\Big) + \\ + \frac{b}{2}\Big(F_{c_1} + F_{c_4} - F_{c_2} - F_{c_3}\Big)\,, \quad (26)$$

where z_{cg} denotes the lever arm of the driving forces with respect to the center of gravity, c.f. Fig. 8 (b),(c).

The moments of inertia in (14),(25),(26) are given by

$$J_{x_{CG}} = \frac{1}{12} m(a^2 + c^2) \quad (27)$$

$$J_{y_{CG}} = \frac{1}{12} m(a^2 + c^2) \quad (28)$$

$$J_{z_{CG}} = \frac{1}{6} m a^2 \quad (29)$$

where a is the width of the slider, c its hight and m its mass.

The complete model of the slider is given by the differential equations (12), (13), (14), (24), (25) and (26) representing the dynamics of the slider in an adequate and simple way.

6. EXPERIMENTAL VERIFICATION

The model derived above was implemented in Simulink and verified using measurements of the test rig. For those experiments the test rig was run in open loop and square-wave input signals with various amplitudes were applied demanding a movement in x-direction. During those experiments the slider was fixed in the y-direction to avoid measurement errors due to disturbances.

Fig. 10 shows the results for $i_{d_x} = 0.1A$, $1A$ and $2A$, respectively. Note that only the position (figures (a_i)) was measured at the test rig. The velocities (b_i) as well as accelerations (c_i) were obtained by numerical differentiation. Moreover, the air gaps in Fig. 10 (d_i) are simulative results only as no sensors for the air gaps are available at the test rig.

By examination of the Figures $(a_{2,3})$, $(b_{2,3})$, $(c_{2,3})$ of the second and the third measurement one can observe that for currents $i_{d_x} > 1A$ the overall mathematical model approximates the real system quite good. However, Fig. 10 (a_1)-(c_1) depicting the results of the first measurement illustrates that there is some kind of damping effect present at low currents ($i_{d_x} < 1A$). The velocity (a_2) increases rapidly at the beginning (0-0.5s) but decreases around 0.5s and settles in a steady-state. Those damping effects might be caused by eddy-current and magnetization effects as observed in [6]. Another possible reason for this behaviour may be due to errors in the commutation or the geometrical assembly of the permanent magnets. Our derived model does not account for any of these effects and thus is not capable to reflect this damping behaviour. Extending the model in this regard will be subject of future investigations.

Fig. 10 $(d_{1,2,3})$ show the simulation results of the air gaps at two of the bearings for an input amplitude of $3A$. The variations of the air gap due to the acceleration in x-direction are very small (in the range of $0.07\mu m$), which is deemed to have no impact on the electromagnetic coupling. The resulting pitch and roll motion are also small such that their influence on the dynamics of the slider is indeed arguable.

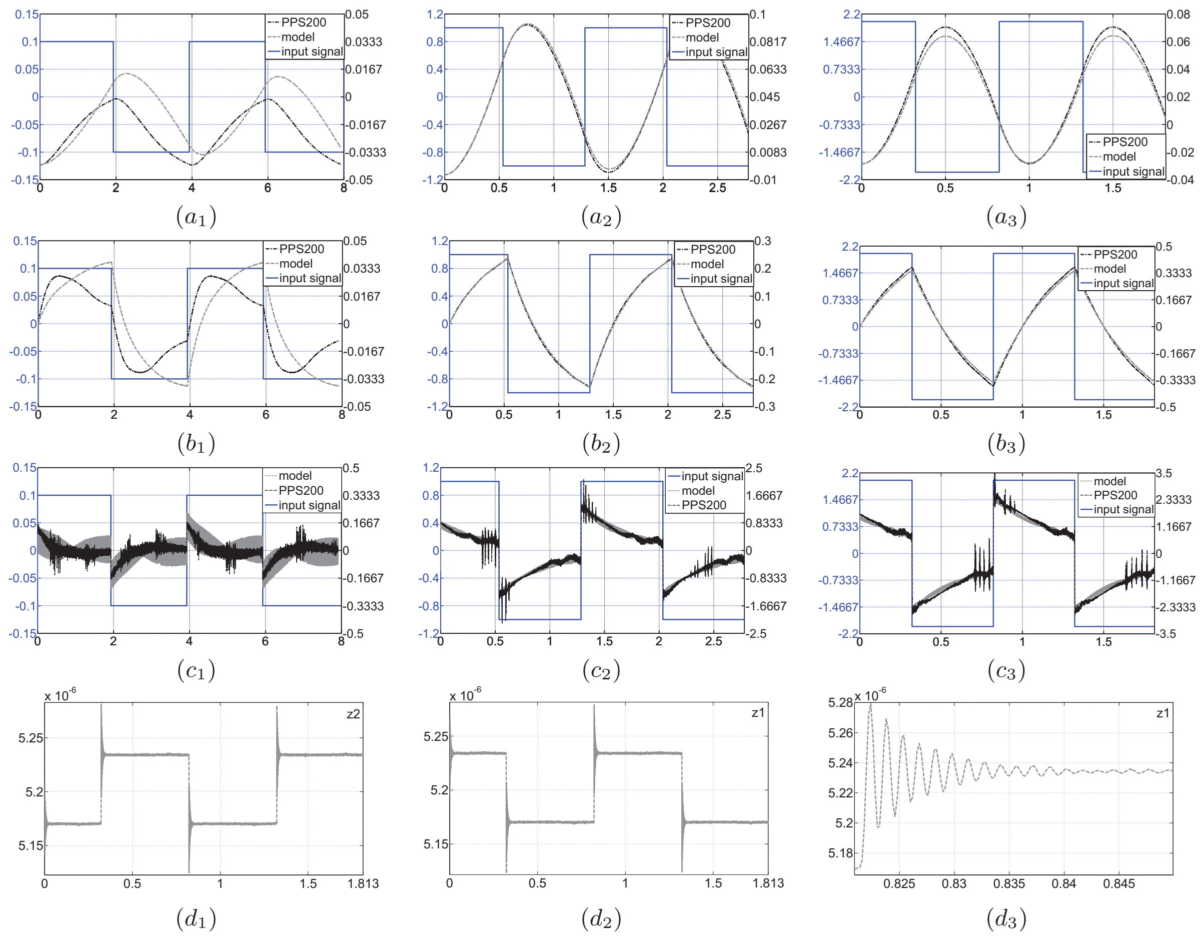

Fig. 10. Experimental and simulation results for $i_{d_x} = 0.1A$ (first column) $i_{d_x} = 1A$ (second), $i_{d_x} = 2A$ (third). Subfigures (a_i): slider position x $[m]$; Subfigures (b_i): velocity $\dot{x}$ $[m/s]$, Subfigures (c_i): acceleration $\ddot{x}$ $[m/s^2]$; Subfigures $(d_{1,2,3})$: air gaps z_2 and z_1, $[m]$ for experiment 3 only.

7. CONCLUDING REMARKS

In this paper we present a study on the dynamic behaviour of Tetra's high-precision planar positioning system "PPS200". We derived physical models of the main components of the system and analysed various nonlinear effects. The resulting system description proves suitable to simulate the dynamics of the positioning system to a large degree of precision. Significant deviations of the simulation and experimental results are only observable at very low input currents. Further investigations are needed to analyse the cause of the damping effect observed for this input range. The derived model is suitable to serve as a basis for analysis and application of nonlinear control algorithms.

8. REFERENCES

[1] Y. Tomita, Y. Koyanagawa, and F. Satoh, "A surface motor-driven precise positioning system," *Precision Engineering*, vol. 16, no. 3, pp. 184–191, 1994.

[2] R.S. Fearing, "A planar milli-robot system on an air bearing," in *7th Int. Symp. Robotics Research*. 1996, vol. 7, pp. 570–581, Springer.

[3] S.Q. Lee and D.G. Gweon, "A new 3-DOF Z-tilts micropositioning system using electromagnetic actuators and air bearings," *Precision Engineering*, vol. 24, no. 1, pp. 24–31, 2000.

[4] W. Gao, S. Dejima, H. Yanai, K. Katakura, S. Kiyono, and Y. Tomita, "A surface motor-driven planar motion stage integrated with an $XY\theta_Z$ surface encoder for precision positioning," *Precision Engineering*, vol. 28, no. 3, pp. 329–337, 2004.

[5] M. Stubenrauch, A. Albrecht, W. Hild, O. Mollenhauer, B. Guddei, S. Spiller, C. Schaeffel, M. Katzschmann, and F. Spiller, "Novel precision positioning system with integrated planar guides," in *53rd International Scientific Colloquium (IWK 2008)*, Ilmenau, Germany, 2008, pp. 251–252.

[6] St. Hesse, H.-U. Mohr, and C. Schaeffel, "Planar motion system for a nanopositioning- and nanomeasuring machine (npmm, nmm) with 200x200m operating range," in *euspen 4th International Conference*, Glasgow, Scotland, 2004.

[7] J.N. Chiasson, *Modeling and high performance control of electric machines*, Wiley-IEEE Press, 2005.

[8] St. Hesse, C. Schaeffel, M. Katzschmann, T. Maass, and H.-U. Mohr, "Planar motor concept for positioning with nanometer position uncertainty," in *euspen 8th International Conference*, Zürich, Switzerland, 2008.